Atmospheric
Chemistry
and Physics

Open Access

Local impact of solar variation on NO_2 in the lower mesosphere and upper stratosphere from 2007 to 2012

F. Friederich[1], M. Sinnhuber[1], B. Funke[2], T. von Clarmann[1], and J. Orphal[1]

[1]Karlsruhe Institute of Technology, Institute for Meteorology and Climate Research, Karlsruhe, Germany
[2]Instituto de Astrofísica de Andalucía, CSIC, Granada, Spain

Correspondence to: F. Friederich (felix.friederich@kit.edu)

Abstract. MIPAS/ENVISAT data of nighttime NO_2 volume mixing ratios (VMR) from 2007 until 2012 between 40 km and 62 km altitude are compared with the geomagnetic Ap index and solar Lyman-α radiation. The local impact of variations in geomagnetic activity and solar radiation on the VMR of NO_2 in the lower mesosphere and upper stratosphere in the Northern Hemisphere is investigated by means of superposed epoch analysis. Observations in the Northern Hemisphere show a clear 27-day period of the NO_2 VMR. This is positively correlated with the geomagnetic Ap index at 60–70° N geomagnetic latitude but also partially correlated with the solar Lyman-α radiation. However, the dependency of NO_2 VMR on geomagnetic activity can be distinguished from the impact of solar radiation. This indicates a direct response of NO_x (NO + NO_2) to geomagnetic activity, probably due to precipitating particles. The response is detected in the range between 46 km and 52 km altitude. The NO_2 VMR epoch maxima due to geomagnetic activity is altitude-dependent and can reach up to 0.4 ppb, leading to mean production rates of 0.029 ppb (Ap d)$^{-1}$. Observations in the Southern Hemisphere do not have the same significance due to a worse sampling of geomagnetic storm occurances. Variabilities due to solar variation occur at the same altitudes at 60–70° S geomagnetic latitude but cannot be analyzed as in the Northern Hemisphere. This is the first study showing the direct impact of electron precipitation on NO_x at those altitudes in the spring/summer/autumn hemisphere.

1 Introduction

Electrons of the aurora and the radiation belts can precipitate into the thermosphere, mesosphere, and even down to the upper stratosphere (Berger et al., 1970; Fang et al., 2008; Clilverd et al., 2010). They need relativistic energies ($\sim$1–4 MeV) to intrude into the lower mesosphere/upper stratosphere (Turunen et al., 2009). Precipitating electrons can ionize or dissociate atmospheric N_2, and subsequent (ion-)chemical reactions lead to an effective NO_x production (Porter et al., 1976; Rusch et al., 1981; Sinnhuber et al., 2012).

Auroral NO production is well known in the thermosphere (e.g., Siskind et al., 1989), whereas the significance of NO_x production due to electron precipitation in the mesosphere and stratosphere is still unclear. Renard et al. (2006) found an increase in stratospheric NO_2 in January–April 2004, supposing that the origin is caused by magnetospheric electrons, but Funke et al. (2007) showed that wintertime downward transport of thermospheric air was the more likely cause of NO_x enhancement in this case. Clilverd et al. (2009) showed a significant response of NO_2 VMR at 45–70 km altitude at high northern latitudes to electron flux data in February 2004. However, in this case it is also unclear to what extent wintertime downward transport has led to the observed NO_x increase (Sinnhuber et al. (2014)). Newnham et al. (2011) showed a direct nitric oxide response above 70 km due to electron precipitation, but still, a direct response of NO_x below 70 km altitude due to electron precipitation in the spring/summer/autumn hemisphere, where NO_x increases cannot be attributed to subsidence, has not been observed to our knowledge. Thus, it is unclear how much

NO$_x$ is produced directly in the mesosphere and upper stratosphere by electrons. An indirect indication of potential NO$_x$ production, however, might be derived from Verronen et al. (2011) and Andersson et al. (2012), who showed a direct hydroxyl response to electron flux above 50 km.

A major influence on stratospheric and mesospheric NO$_x$ is given by so-called solar proton events (SPE) (Crutzen et al., 1975; Jackman et al., 1980). Proton precipitation leads to an effective NO$_x$ production and can significantly enhance the VMR, e.g., about 50–60 ppb in the lower mesosphere in October–November 2003 (Jackman et al., 2005; López-Puertas et al., 2005).

The NO$_x$ dependency on the solar spectral irradiance variabilities in the upper stratosphere/lower mesosphere has been investigated rarely to our knowledge. Keating et al. (1986) observed a response to the 27-day solar rotation signal in NO$_2$ at low latitudes below 40 km altitude. Hood et al. (2006) found a negative dependency of NO$_x$ anomalies on the Mg II solar UV index at the equatorial stratopause, and a positive dependency at high latitudes at the upper stratosphere and the lower mesosphere using a 12 year data set of the Halogen Occultation Experiment (HALOE). Gruzdev et al. (2009) have searched for the 27-day solar rotation signal in NO and NO$_2$ by means of a 3-D chemistry–climate model study. They have found significant sensitivities below 40 km and above 60 km, but not in between, although a connection with temperature and ozone both depending on solar UV radiation at these altitudes (Austin et al., 2007; Gruzdev et al., 2009) seems plausible.

In this study we analyze NO$_2$, which is the main constituent of NO$_x$ in the upper stratosphere and lower mesosphere during night. For that, we use nighttime data of the nominal mode observations of the Michelson Interferometer for Passive Atmospheric Sounding (MIPAS, Fischer et al., 2008) on the Environmental Satellite (ENVISAT). We use the Ap index provided by the National Geophysical Data Center (http://www.ngdc.noaa.gov) as an indicator of geomagnetic activity, and Lyman-α, provided by the LASP Interactive Solar Irradiance Data Center (LISIRD, http://lasp.colorado.edu/lisird/), as an indicator of solar UV radiation.

2 MIPAS/ENVISAT

Until contact with ENVISAT was lost on 08 April 2012, the MIPAS instrument recorded limb emission spectra of the Earth's atmosphere. Since spring 2002, MIPAS detected many atmospheric trace gases in the infrared region (4.1–14.7 μm) including NO$_2$ by its fundamental ν_3 band (6.2 μm). Due to the sun-synchronous orbit of ENVISAT, MIPAS measured at ∼ 10 a.m. and ∼ 10 p.m. local time. We use nighttime data (solar zenith angle > 96°) of the nominal measurement mode (6–68 km). Data are retrieved by the IMK-IAA processor (von Clarmann et al., 2003). The NO$_2$ retrieval is described in Funke et al. (2005) and has been improved since

then (Funke et al., 2011). We use daily means of the versions V5R_NO2_220 and V5R_NO2_221. The arithmetic mean of the averaging kernel diagonal elements of single observations has to be greater than 0.03 (Funke et al., 2011), in order to take the daily means of NO$_2$ into account.

MIPAS also observes NO that would allow us to analyze the mesospheric response to geomagnetic variability for NO$_x$ (NO+NO$_2$) instead of NO$_2$ alone. However, sensitivity tests have shown that mesospheric NO retrieved during polar summer can be affected by a down-folded thermospheric signal of the same order as the expected local response to geomagnetic variability (∼1 ppb). Thus, small variations of geomagnetic activity affecting thermospheric NO cannot be distinguished in the mesospheric NO signal from the possible local impact on mesospheric NO. Since NO$_2$ is not affected as there is no thermospheric NO$_2$, we only use this gas for data analysis instead of NO$_x$.

3 Data analysis

In this section, we give a short overview of the data we use and the methods of data analysis (Sect. 3.1). We use the superposed epoch analysis method (SEA, Chree et al., 1913), also known as the compositing method (von Storch and Zwiers, 2001), to search for small responses to solar variations. For the Northern Hemisphere, we did SEAs with four different conditions in order to distinguish between the dependence on geomagnetic activity and solar UV radiation (Sect. 3.2). We analyze the SEAs by means of the Pearson correlation coefficient r to determine linear dependencies, and the quadrant correlation (Blomqvist et al., 1950) to determine non-linear, monotone dependencies. Linear least-square fits to the SEAs lead to the determination of the altitude-dependent NO$_x$ lifetime, and the altitude- and Ap index-dependent NO$_x$ production rate (Sect. 3.3). Finally, we performed one SEA for the Southern Hemisphere (Sect. 3.4).

3.1 Method

Figure 1 shows the daily zonal means of nighttime NO$_2$ VMR measured by MIPAS at $65 \pm 5°$ N and $65 \pm 5°$ S geomagnetic latitude, the Ap index, and solar Lyman-α flux in 2007–2012, i.e., during solar minimum (2007–2010) and during solar maximum (2011–2012), as a function of time. Days for analysis were chosen such that the influence of other effects besides solar variabilities, e.g., due to NO$_x$ subsidence in polar winter, is minimized in the Northern Hemisphere. There was no SPE affecting the Earth's atmosphere in the years 2007–2009, but one SPE occurred in 2010, and six SPEs in 2011 (http://www.swpc.noaa.gov). For each SPE the days from the onset until three days after the maximum are excluded. However, this was found to have no significant effect on the results of the paper. On 23–30 January 2012 and 7–15 March 2012 strong SPE occurred, producing NO$_x$ the

Table 1. Time periods for which MIPAS NO_2 data are used in the analysis. The periods left out for Figs. 9 and 10 are in parentheses.

Northern Hemisphere	Southern Hemisphere
21 Mar 2007–28 Oct 2007	13 Sep 2007–07 Apr 2008
05 Apr 2008–05 Oct 2008	(17 Sep 2008–15 Apr 2009)
28 Apr 2009–07 Oct 2009	(02 Sep 2009–30 Mar 2010)
20 Mar 2010–12 Oct 2010	10 Sep 2010–15 Apr 2011
24 Feb 2011–05 Oct 2011	10 Sep 2011–21 Jan 2012

middle atmosphere (von Clarmann et al., 2013). Therefore, we do not use MIPAS data from 23 January 2012 on.

At the chosen time periods (Table 1), 659 daily means of MIPAS NO_2 VMR can be used in the Northern Hemisphere and 697 in the Southern Hemisphere. We restrict our analysis to geomagnetic latitudes from $0°$ to $80°$ of each hemisphere for the following reasons: first, with this restriction, downwelling of NO_x-rich upper atmospheric air of the other hemisphere in polar winter is excluded. Second, because we analyze nighttime data, and our time periods include polar day at high latitudes, there is not sufficient data at geomagnetic latitudes higher than $80°$. We analyze $10°$-zonal means, restricting our analysis to spring/summer/autumn.

A direct correlation of the Ap index and NO_2 VMR does not lead to a significant result. First, this is due to the predominance of the seasonal variability of NO_2. Furthermore, only NO_2 anomalies can be unambiguously assigned to electron fluxes (or UV radiation), because constant electron-induced NO_x production leads to an equilibrium concentration without rapid time dependence. Mid- and long-term variations compete against photochemistry and dynamics and are thus unaccessible to our analysis. Hence, a high-pass filter is applied to NO_2 VMR, Ap index, and Ly-α as outlined in the following.

We assume that the measured NO_2 VMR is composed of two parts: The time-dependent $NO_{2\text{background}}$ VMR that takes mid- and long-term variations into account, and changes due to short-time variabilities, ΔNO_2. $NO_{2\text{background}}$ is determined by a 27-day running mean representing a rectangular filter, shown as a red curve in Fig. 1 (top). In the same way, we determine variabilities of geomagnetic activity and solar radiation, i.e., $X = (NO_2, Ap, Ly-\alpha)$:

$$\Delta X = X_{\text{measured}} - X_{\text{background}}. \quad (1)$$

To show similarities in the short-term behavior of ΔNO_2, ΔAp and $\Delta Ly-\alpha$, we use the superposed epoch analysis (SEA) method, introduced by Chree et al. (1913), also known as the compositing method (von Storch and Zwiers, 2001). We define four classes of epochs. Each epoch is a time interval of ± 30 days around day d. Days are considered, when Ap index and/or solar Ly-α fluxes fulfill particular conditions on day d as specified below. Furthermore, only days are considered where MIPAS NO_2 nighttime measurements are avail-
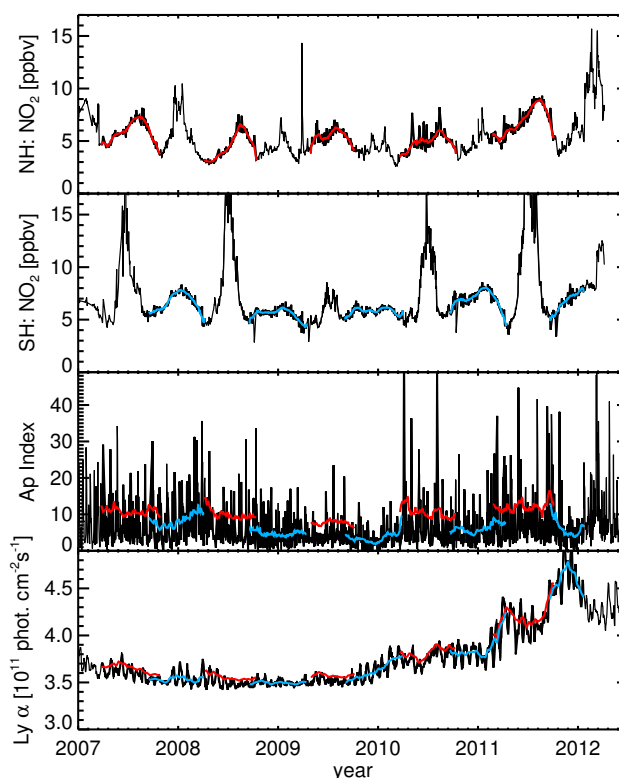

Fig. 1. First panel: Daily means of nighttime NO_2 VMR in ppb at $65 \pm 5°$ N geomagnetic latitude and 50 km altitude in 2007–2012. Second panel: The same for $65 \pm 5°$ S geomagnetic latitude. The red/blue curve shows the 27-day running mean of the curve for the days listed in Table 1. Third panel: Daily means of the Ap index in 2007–2012. The blue curve shows the 27-day running mean of the curve for the days listed in the SH column in Table 1. The red curve shows the same for the days listed in the NH column, shifted by 3.5 for the days defining the threshold of an Δ Ap event. Fourth panel: Solar Lyman-α in 2007–2012. The blue curve shows the 27-day running mean of the curve for the days listed in the SH column in Table 1. The red curve shows the same for the days listed in the NH column, shifted by 0.05 photons cm^{-2} s^{-1} defining the threshold of an Δ Lyman-α event.

able. It is possible that the same event can be counted in different epochs at, e.g., days –27, 0, and 27, but if some events are counted several times, they will be counted for the ΔAp, ΔLy-α, and ΔNO_2 epochs, so the same averaged epochs are compared.

- *Epoch type 1.* $\Delta Ap > 3.5$ (shown by the red curve in Fig. 1, middle), to see the correlation between the signals of ΔNO_2 and ΔAp. The criterion is chosen in that way so that there are ∼100 different epochs to count in the Northern Hemisphere.

- *Epoch type 2.* $\Delta Ap > 3.5$ and $|\Delta Ly-\alpha| < 0.015$ photons cm^{-2} s^{-1}, in order to exclude UV radiation as a source of NO_x variation from epoch type 1.
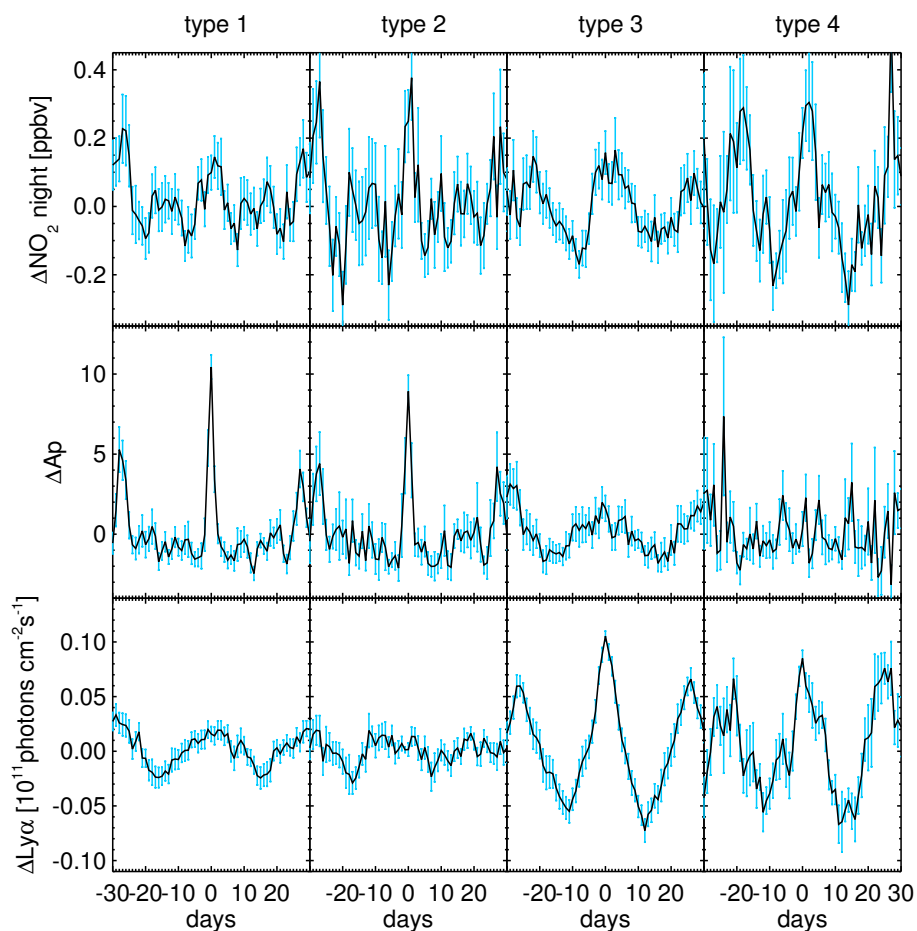
Fig. 2. SEAs of 103/34/96/21 (epoch types 1/2/3/4, respectively) different events in 2007–2011 at 50 km altitude and 65 ± 5° N geomagnetic latitude. The columns define the epoch type number, the rows show Δ NO$_2$, Δ Ap, and Δ Ly-α. The blue error bars show the 1σ range.

– *Epoch type 3.* Δ Ly-$\alpha > 0.05 \times 10^{11}$ photons cm^{-2} s^{-1} (shown by the red curve in Fig. 1, bottom), to see the correlation between the signals of Δ NO$_2$ and Δ Ly-α.

– *Epoch type 4.* Δ Ly-$\alpha > 0.05 \times 10^{11}$ photons cm^{-2} s^{-1} and $|\Delta$ Ap$| < 1.0$, in order to exclude particle precipitation as a source of NO$_x$ production from epoch type 3.

Events at day d are defined by the variations of the Ap index/solar Lyman-α flux and not by their absolute values for the following reasons. First, a fixed threshold cannot define each single event in a 5 yr period due to long-term variations of the indices. Second, short-term variations in NO$_2$ are supposed to occur with short-term variations of the indices rather than exceeding a threshold, with only little change in the absolute value due to mid- or long-term variations. These are in competition with photochemistry and dynamics and not verifiable with the SEA.

The thresholds are chosen in this way so that on the one hand the sample of events/epochs is sufficiently large, on the other hand as high as possible. In the Northern Hemi-

sphere, we obtain the following number of events $N = 103/34/96/21$ for epoch types 1/2/3/4, respectively. These N time series of the quantities $q = (\Delta$ NO$_2, \Delta$ Ap, Δ Ly-$\alpha)$, each 61 days long, are co-added

$$\overline{q}_i = \frac{\sum_{j=1}^{M_i} q_{i,j}}{M_i}, i = [1, 61], \tag{2}$$

i.e., averaged under consideration of their phase with respect to the Δ Ap/Δ Ly-α event, which is called SEA. Due to gaps in the time series of NO$_2$ VMR, the number of summands M_i at each phase point i is lower than the number of epochs N (roughly $M_i \simeq 0.7 \cdot N$).

3.2 Northern Hemisphere: different epoch types

The SEA is exemplified in Fig. 2 as a black curve at 50 km altitude and 65 ± 5° N geomagnetic latitude for Δ NO$_2$, Δ Ap, and Δ Ly-α and for all four epoch types. The blue error bars show the 1σ standard error of the mean of each value in all figures. In the following, we describe the different epoch

types in detail, for each starting with the conditions mentioned in Sect. 3.1.

Epoch type 1, ΔAp > 3.5, $N = 103$: There are sharp peaks around days -27, 1, and 28 at ΔNO$_2$, around days -27, 0, and 27 at ΔAp, and broad peaks at ΔLy-α with maxima on the same days. This is consistent with the average solar rotation. There is roughly the same peak value at days -27, 0, and 27 at ΔNO$_2$ and ΔLy-α, but different peak values at ΔAp. This together with the broadening of the ΔNO$_2$ peak indicates the influence of the UV radiation. There are distinct but insignificant small maxima between days -27, 0, and 27. They are triggered by high UV radiation averaged out in the ΔLy-α epoch of the figure, but due to non-linear influences of UV radiation on ΔNO$_2$, which are explained below, the observed small and non-significant maxima can appear.

Epoch type 2, ΔAp > 3.5 and $|\Delta$Ly-$\alpha| <$ 0.015 photons cm^{-2} s^{-1}, $N = 34$: The significant correlation between ΔAp and ΔNO$_2$ is more pronounced, if variations in ΔLy-α are suppressed. The 27-day period is clearly visible. Here, the central peak at day 1 is even higher than those one period before and after. Evidently, the averaged NO$_2$ enhancement is linked to the ΔAp peaks, which are an indicator of enhanced particle precipitation. The out-of-phase UV-radiation signal appears faintly at ΔNO$_2$ with a broad maximum around day -10.

Epoch type 3, ΔLy-$\alpha > 0.05 \times 10^{11}$ photons cm^{-2} s^{-1}, $N = 96$: There are broad peaks around days -27, 0, and 27 at ΔNO$_2$, ΔAp, and ΔLy-α and the correlation between ΔLy-α, and ΔNO$_2$ is noticeably good. Additionally, the correlation between ΔAp and ΔNO$_2$ is also very good.

Epoch type 4, ΔLy-$\alpha > 0.05 \times 10^{11}$ photons cm^{-2} s^{-1} and $|\Delta$Ap$| < 1.0$, $N = 21$: The ΔAp signal does not show a 27-day period. Instead it is more noisy due to smaller N. The ΔNO$_2$ signal is not as smooth as in epoch type 3, due to the smaller N and due to a noisy ΔAp signal. Both epoch types 3 and 4 show that changes in the UV flux have a significant impact on NO$_2$, probably triggered by the response of ozone and temperature to UV flux changes at these altitudes (e.g., Austin et al., 2007), throughout the 27-day cycle. Thus, again, we have to consider the impact of UV radiation while searching for the one of particle precipitation.

As discussed above, in epoch type 2, only very small UV radiation variations are permitted. The correlation coefficient r of that epoch type between ΔAp and ΔNO$_2$ is shown for all calculated altitudes and geomagnetic latitudes in Fig. 3 ($10° \times 2$ km grid). The three panels (top/middle/bottom) show the resultant r when the ΔNO$_2$ signal has a delay of 0/1/2 days, respectively. The correlation coefficient is highest (greater than 0.6) at geomagnetic latitudes of the outer radiation belt at $65 \pm 5°$ N and one day delay. The central peak of the ΔNO$_2$ SEA also appears on day 1. There is neither a significant correlation at lower geomagnetic latitudes nor at $75 \pm 5°$ N.
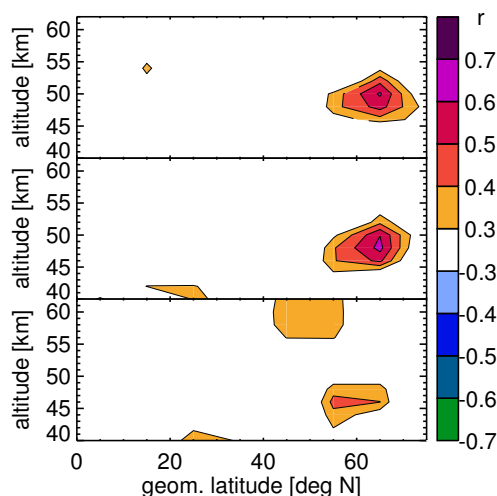

Fig. 3. Correlation coefficient r of the SEA with respect to ΔAp (epoch type 2) between ΔAp and ΔNO$_2$, plotted over geomagnetic latitudes with 0/1/2 days delay (top/middle/bottom, respectively).
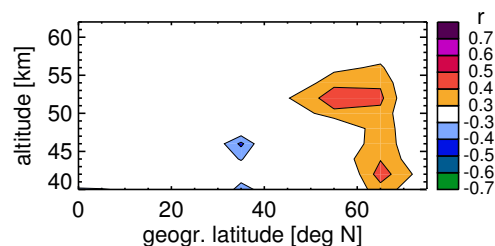

Fig. 4. Correlation coefficient r of the SEA with respect to ΔAp (epoch type 2) between ΔAp and ΔNO$_2$ with a delay of one day, plotted over geographic latitudes.

We also calculated epoch type 2 for geographic zonal means. The correlation coefficients for a delay of one day in ΔNO$_2$ are shown in Fig. 4. They become significantly lower at high northern latitudes. Consequently, Figs. 3 and 4 point out that the observed NO$_x$ is dependent on high northern geomagnetic latitudes and not on geographic latitudes. This is another hint at the local impact of electron precipitation.

Even though a dependence of ΔNO$_2$ on ΔLy-α is clearly visible in the SEA, linear dependency cannot be assumed due to several simultaneous influences. UV radiation has an impact on the temperature, ozone, the ozone column above, and on the NO photolysis rate, for example, each resulting in variations of the NO$_2$ VMR at night. Thus we need a method which is able to detect also nonlinear correlations. We have chosen the quadrant correlation (Blomqvist et al., 1950), which requires only that the relation between two variables is monotonic. By this method, the precision p is determined, indicating the significance level of a monotonic correlation between both variables. p does not determine the strength of the correlation or the sign of the monotonicity.
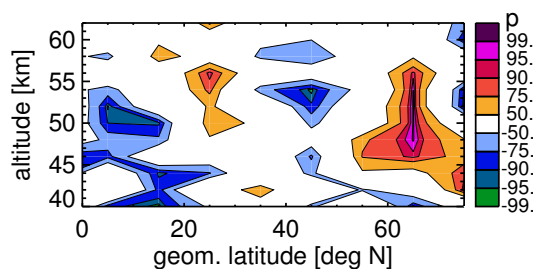
Fig. 5. Altitude- and geomagnetic latitude-dependent precision p of the quadrant correlation of Δ Ly-α and Δ NO$_2$. The sign indicates whether the correlation is positive or negative.
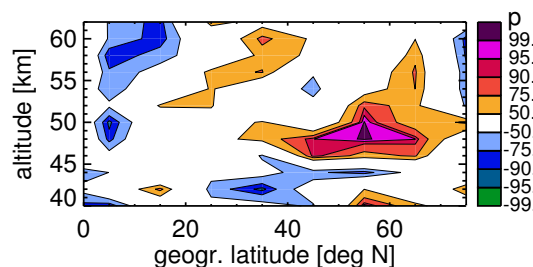

Fig. 6. Same as Fig. 5 but with geographic latitudes.

Here, every daily mean is considered, subject to the condition that $|\Delta \text{Ap}| < 1.0$ is true for a certain day and the day before.

In Fig. 5, the quadrant correlation is plotted over geomagnetic latitudes, and in Fig. 6 over geographic latitudes, respectively. The color code shows both p and the sign of the correlation. Figure 5 shows a positive correlation at $65 \pm 5°$ N geomagnetic latitude, which could be caused by electron precipitation in phase with solar Lyman-α flux, not filtered out by the Ap index criterion. In Fig. 6, there is a strong correlation at 45–65° N and 48–50 km altitude. It could be partly a blurred effect of the positive correlation appearing in geomagnetic latitudes, but since p is even higher, other effects have to be taken into account. Simultaneous variations in temperature, ozone, and NO photolysis triggered by UV radiation can affect Δ NO$_2$ as well. This can lead to a positive correlation at high latitudes and a negative correlation at lower latitudes.

However, the detailed analysis of the UV-radiation response is beyond the scope of the paper. In the following, it is only essential that the UV-radiation response does not affect the Ap response, which is the case for epoch type 2.

3.3 Northern Hemisphere: fit to the SEA

In order to determine an Ap index-dependent NO$_x$ production rate we fit a simple model to the epoch type 2 SEAs of Δ NO$_2$ at $65 \pm 5°$ N geomagnetic latitude. We account for a linear dependency of the Ap index, namely the NO$_x$ production rate per day pr, and the altitude-dependent NO$_x$ lifetime τ. Since we analyze NO$_2$ at a fixed local times (and
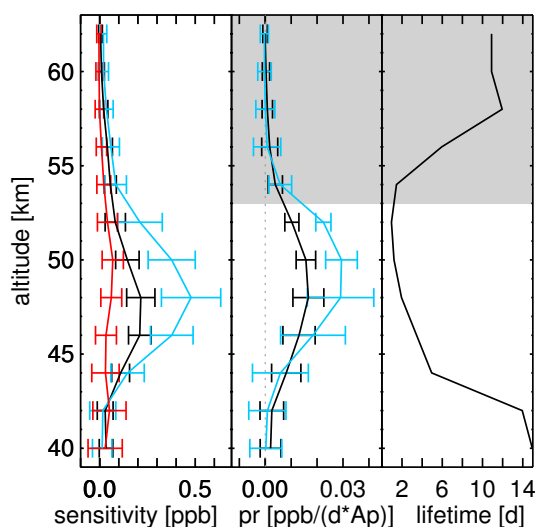

Fig. 7. Left: Altitude-dependent sensitivity of Δ NO$_2$ on the conditions of epoch types 1/2/3 shown in black/blue/red, respectively. Middle: Altitude-dependent production rate pr or epoch type 1/2 shown in black/blue, respectively. Right: Altitude-dependent Δ NO$_2$ lifetime at night. All quantities were determined at $65 \pm 5°$ N geomagnetic latitude. The error bars show the 1σ range. The shadowed area marks the altitudes, where the determination of the lifetime is not reliable.

hence roughly constant NO$_x$ partitioning), retrieved NO$_2$ lifetimes correspond to NO$_x$ lifetimes. Effects of the rectangular filter we use to determine NO$_{2\text{background}}$ are insignificant. As a first step, we determine pr and τ iteratively by minimizing the residual:

$$\chi^2 = \sum_{i=0}^{60} \left(\frac{\sum_{t=0}^{T} e^{\frac{-t}{\tau}} \cdot pr \cdot \Delta \text{Ap}_{i-t} - \Delta \text{NO}_{2i}}{\sigma_i} \right)^2 . \quad (3)$$

T denotes an integer depending on τ (typically $\sim 2 - 3 \cdot \tau$). σ_i denotes the variance of ΔNO_{2i}. In Fig. 7 (right), τ is plotted in dependence on the altitude. At altitudes higher than 54 km, τ becomes most likely lower than one day, but the analysis of daily means is not able to resolve that. This is why the figure is shadowed at these altitudes. The Δ NO$_2$ lifetimes are significantly lower at all altitudes than the NO$_x$ lifetimes after an SPE determined by Friederich et al. (2013). τ is mostly triggered by dynamics at these altitudes (Brasseur and Solomon, 2005; Friederich et al., 2013). At an SPE, NO$_x$ is enhanced over the whole polar cap, whereas NO$_x$ enhancement due to electron precipitation is restricted to a small region. Due to mixing with air that was not affected by electron precipitation the dynamical lifetime of NO$_x$ is significantly lower than after a SPE.

In order to determine pr precisely together with its variance, we applied a least squares fit utilizing τ determined before. In Fig. 7 (middle), pr is plotted with its 1σ range in dependence on altitude. The black curve shows the result for epoch type 1, the blue one for epoch type 2. The Δ NO$_2$
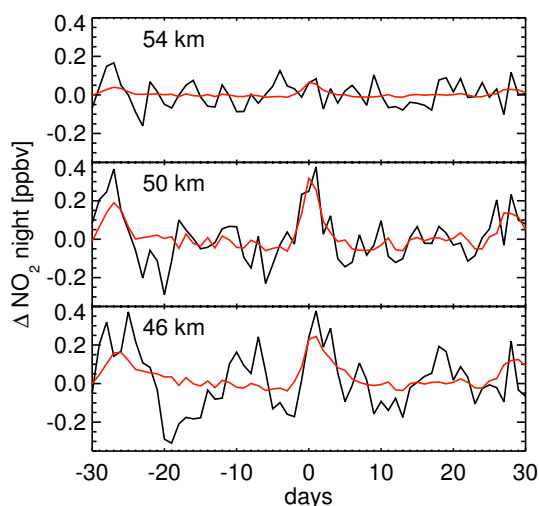
Fig. 8. SEA of Δ NO$_2$ at $65 \pm 5°$ N geomagnetic latitude and different altitudes (black). In red the corresponding fits.

Fig. 9. Epoch type 1 SEA of Δ NO$_2$ at $65 \pm 5°$ S geomagnetic latitude and 50 km altitude. The blue error bars show the 1σ range.

value at day 1, hereinafter called sensitivity, of the epoch types 1/2/3 is shown as a black/blue/red curve, respectively, in the left column of Fig. 7.

Below 44 km there is neither any signal in the sensitivity nor in the production rate. Thus, 44 km is the lower boundary, where electron precipitation can be detected with NO$_2$ measurements of MIPAS in 2007–2011. The sensitivity maximizes at 48 km at 0.20/0.41 ppb for epoch types 1 and 2, respectively, while the production rate maximizes at 50 km at 0.015/0.029 ppb (Ap d)$^{-1}$. The difference in altitude can be explained by the different NO$_x$ lifetimes. At altitudes higher than 52 km there is neither any significant sensitivity nor any positive production rate. This is most probably due to the fact that the NO$_x$ lifetime is lower than one day making it impossible to detect it by analyzing daily means. Nevertheless, it should be considered that the NO$_2$/NO$_x$ ratio decreases with increasing altitude at night. Additionally, the efficiency of NO$_x$ production due to ionization, which is mainly influenced by temperature-dependent reactions, shows its peak between 42 km and 52 km (Funke et al., 2011; Friederich et al., 2013). These two reasons could also explain the decrease in the production rate from 50 km to 52 km. In Fig. 8, the averaged epochs of epoch type 2 at 54, 50, and 46 km altitude are shown in black (top/middle/bottom, respectively). The fits to each of them are shown in red. These fits illustrate that the central peak and the peaks around days ± 27 can be explained by an Ap index-dependent NO$_x$ production considering the altitude-dependent NO$_x$ lifetime.

3.4 Southern Hemisphere

We performed the same analysis for the Southern Hemisphere at the time periods as described in Table 1. It turned out that applying the 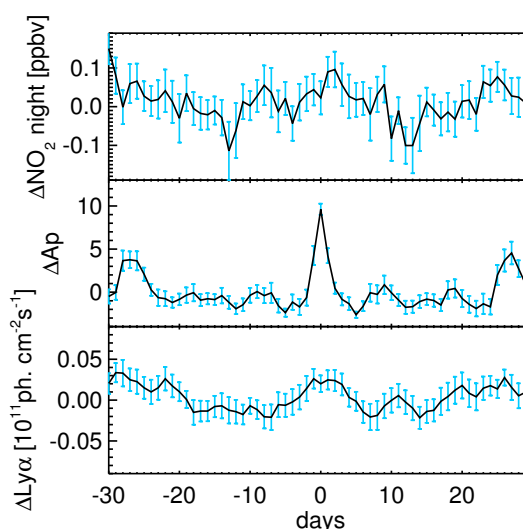criteria of the different epoch types to the whole data set did not lead to any significant results. The reason for that is the sampling of the Ap index. Ap events are generally lower during the periods of polar summer in the Southern Hemisphere used for the analysis, especially in the southern summers of 2008/2009 and 2009/2010. The Ap index is so low during these periods that it has no significant effect on Δ NO$_2$, and other variations perturb the SEA. Therefore, these two periods are taken out of the analysis. There are 372 daily means of MIPAS measurements left. Applying epoch type 1 leads to 68 events.

In Fig. 9, the SEA of epoch type 1 is shown for $65 \pm 5°$ S geomagnetic latitude and 50 km altitude. The maximum values around 0.1 ppb of Δ NO$_2$ are at days 1 and 2, but the peak is very broad. The other maxima are at day –26 and at day 25. The minima are at days –13 and 13. A 27-day cycle is slighty identifiable, but the width of the peaks and the relative errors are larger than in the Northern Hemisphere. This is due to the lower number of used measurements and due to the worse sampling of the Ap index in the periods. Thus, SEAs of the other epoch types and a correlation analysis do not lead to any significant result. In Fig. 10 the sensitivity of Δ NO$_2$ at day 1 is shown. Maximum values are 0.09 ppb at 48 and 50 km altitude. The altitudes with the highest sensitivity and the shape of the curve are similar to the Northern Hemisphere and confirm the results of Sect. 3.2 and 3.3. The maximal values are lower due to the reasons already mentioned.

4 Conclusions

We showed the significant influence of solar variabilities on nighttime NO$_2$ and consequently on NO$_x$ in the lower mesosphere and upper stratosphere during solar minimum and the
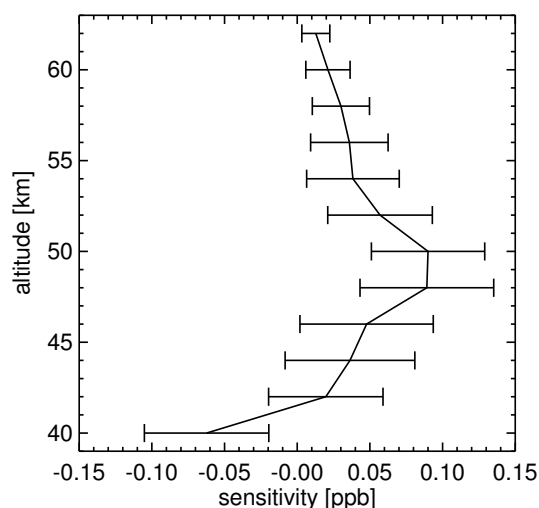
Fig. 10. Altitude-dependent sensitivity of Δ NO$_2$ to the conditions of epoch type 1 at $65 \pm 5°$ S geomagnetic latitude.

beginning of solar maximum. The 27-day period is clearly visible in Δ NO$_2$ generated by short-time variabilities in solar UV radiation and electron precipitation. We have distinguished the geomagnetic influence from that of UV radiation at 60–70° N geomagnetic latitude. This distinction and the fact that there is only a signal at geomagnetic latitudes of the outer radiation belt lead to the conclusion that electron precipitation is a source of NO$_x$ production in the lower mesosphere and upper stratosphere.

The MIPAS nighttime NO$_2$ signal shows a delay of one day to the Ap index. Likewise, other studies have shown a delay of one day of the auroral NO production compared to auroral activity between 100 km and 160 km (Solomon et al., 1999; Marsh et al., 2004). Newnham et al. (2011) see a 1–2 day delay of enhanced NO, with respect to the > 30 keV and > 300 keV electron flux at altitudes between 70 km and 85 km. Thus, the MIPAS NO$_2$ observations in the lower mesosphere and upper stratosphere are consistent with previous NO observations in the upper mesosphere and lower thermosphere but are of considerably lower magnitude.

The correlation coefficient r between the SEAs of Δ Ap and Δ NO$_2$ is greater than 0.4 between 44 km and 52 km altitude. Andersson et al. (2012) showed that the correlation coefficients of single events between daily mean OH and daily mean 100–300 keV electron count rates are greater than 0.35 down to 52 km. They did not find a clear correlation below. The NO$_2$ enhancement due to electron impact shown in this study is low but significant. Altitude-dependent production rates were determined maximizing at 0.029 ppb $(A$ p d$)^{-1}$ at 50 km altitude. Above, the decrease of the signal with altitude could be explained by a decrease in the nighttime NO$_2$/NO$_x$ ratio with increasing altitude, with the efficiency of NO$_x$ production, and mainly with the altitude-dependent NO$_x$ lifetime.

Observations in the Southern Hemisphere are less significant due to a worse sampling of the Ap index during the analyzed time periods. Nevertheless, they show a slight 27-day cycle and confirm that the altitudes of maximal sensitivity of NO$_2$ to solar variation are 48–50 km.

This is the first study showing the independent influence of electron precipitation on NO$_2$, and on trace gases in general, at altitudes between 46 km and 52 km in the spring/summer/autumn hemisphere to our knowledge. Further studies are necessary to investigate the possible impact on ozone and examine the NO$_x$ production rates during solar maximum.

References

Andersson, M. E., Verronen, P. T., Wang, S., Rodger, C. J., Clilverd, M. A., and Carson, B. R.: Precipitating radiation belt electrons and enhancements of mesospheric hydroxyl during 2004–2009, J. Geophys. Res., 117, D09304, doi:10.1029/2011JD017246, 2012.

Austin, J., Hood, L. L., and Soukharev, B. E.: Solar cycle variations of stratospheric ozone and temperature in simulations of a coupled chemistry-climate model, Atmos. Chem. Phys., 7, 1693–1706, 10,
http://www.atmos-chem-phys.net/7/1693/10/.5194/acp-7-1693-2007, 2007.

Berger, M. J., Seltzer, S. M., and Maeda, K.: Energy deposition by auroral electrons in the atmosphere, J. Atmos. Terr. Phys., 32, 1015–1045, 1970.

Blomqvist, N.: On a measure of dependence between two random variables, Ann. Math. Statist., 21, 593–601, 1950.

Brasseur, G. P. and Solomon, S.: Aeronomy of the Middle Atmosphere, 3rd edn., Springer, Dordrecht, the Netherlands, 341–346, 2005.

Chree, C.: Some Phenomena of Sunspots and of Terrestrial Magnetism at Kew Observatory, Philos. T. Roy. Soc. Ldn., 212, 75–116, 1913.

Clilverd, M. A., Seppälä, A., Rodger, C. J., Mlynczak, M. G., and Kozyra, J. U.: Additional stratospheric NO$_x$ production by relativistic electron precipitation during the 2004 spring NO$_x$ descent event, J. Geophys. Res., 114, A04305, doi:10.1029/2008JA013472, 2009.

Clilverd, M. A., Rodger, C. J., Gamble, R. J., Ulich, T., Raita, T., Seppälä, A., Green, J. C., Thomson, N. R., Sauvaud, J.-A., and Parrot, M.: Ground-based estimates of outer radiation belt energetic electron precipitation fluxes into the atmosphere, J. Geophys. Res., 115, A12304, doi:10.1029/2010JA015638, 2010.

Crutzen, P. J., Isaksen, I. S. A., and Reid, G. C.: Solar proton events – stratospheric sources of nitric oxide, Science, 189, 457–459, doi:10.1126/science.189.4201.457, 1975.

Fang, X., Randall, C. E., Lummerzheim, D., Solomon, S. C., Mills, M. J., Marsh, D. R., Jackmann, C. H., Wang, W., and Lu, G.: Electron impact ionization: A new parameterization for 100 eV to 1 MeV electrons, J. Geophys. Res., 113, A09311, doi:10.1029/2008JA013384, 2008.

Fischer, H., Birk, M., Blom, C., Carli, B., Carlotti, M., von Clarmann, T., Delbouille, L., Dudhia, A., Ehhalt, D., Endemann, M., Flaud, J. M., Gessner, R., Kleinert, A., Koopman, R., Langen, J., López-Puertas, M., Mosner, P., Nett, H., Oelhaf, H., Perron, G., Remedios, J., Ridolfi, M., Stiller, G., and Zander, R.: MIPAS: an instrument for atmospheric and climate research, Atmos. Chem. Phys., 8, 2151–2188, doi:10.5194/acp-8-2151-2008, 2008.

Friederich, F., von Clarmann, T., Funke, B., Nieder, H., Orphal, J., Sinnhuber, M., Stiller, G. P., and Wissing, J. M.: Lifetime and production rate of NO$_x$ in the upper stratosphere and lower mesosphere in the polar spring/summer after the solar proton event in October–November 2003, Atmos. Chem. Phys., 13, 2531–2539, doi:10.5194/acp-13-2531-2013, 2013.

Funke, B., López-Puertas, M., von Clarmann, T., Stiller, G. P., Fischer, H., Glatthor, N., Grabowski, U., Höpfner, M., Kellmann, S., Kiefer, M., Linden, A., Mengistu Tsidu, G., Miliz, M., Steck, T., and Wang, D. Y.: Retrieval of stratospheric NO$_x$ from 5.3 and 6.2 μm nonlocal thermodynamic equilibrium emissions measured by Michelson Interferometer for Passive Atmospheric Sounding (MIPAS) on Envisat, J. Geophys. Res., 110, D09302, doi:10.1029/2004JD005225, 2005.

Funke, B., López-Puertas, M., Fischer, H., Stiller, G. P., von Clarmann, T., Wetzel, G., Carli, B., and Belotti, C.: Comment on "Origin of the January–April 2004 increase in stratospheric NO₂ observed in the northern polar latitudes", Geophys. Res. Lett., 34, L07813, doi:10.1029/2006GL027518, 2007.

Funke, B., Baumgaertner, A., Calisto, M., Egorova, T., Jackman, C. H., Kieser, J., Krivolutsky, A., López-Puertas, M., Marsh, D. R., Reddmann, T., Rozanov, E., Salmi, S.-M., Sinnhuber, M., Stiller, G. P., Verronen, P. T., Versick, S., von Clarmann, T., Vyushkova, T. Y., Wieters, N., and Wissing, J. M.: Composition changes after the "Halloween" solar proton event: the High Energy Particle Precipitation in the Atmosphere (HEPPA) model versus MIPAS data intercomparison study, Atmos. Chem. Phys., 11, 9089–9139, doi:10.5194/acp-11-9089-2011, 2011.

Gruzdev, A. N., Schmidt, H., and Brasseur, G. P.: The effect of the solar rotational irradiance variation on the middle and upper atmosphere calculated by a three-dimensional chemistry-climate model, Atmos. Chem. Phys., 9, 595–614, doi:10.5194/acp-9-595-2009, 2009.

Jackman, C. H., Frederick, J. E., and Stolarski, R. S.: Production of odd nitrogen in the stratosphere and mesosphere: An intercomparison of source strengths, J. Geophys. Res., 85, 7495–7505, doi:10.1029/JC085iC12p07495, 1980.

Jackman, C. H., DeLand, M. T., Labow, G. J., Fleming, E. L., Weisenstein, D. K., Ko, M. K. W., Sinnhuber, M., and Russell, J. M.: Neutral atmospheric influences of the solar proton events in October–November 2003, J. Geophys. Res., 110, A09S27, doi:10.1029/2004JA010888, 2005.

Hood, L. L. and Soukharev, B. E.: Solar induced variations of odd nitrogen: Multiple regression analysis of UARS HALOE data, J. Res. Lett., 33, L22805, doi:10.1029/2006GL028122, 2006.

Keating, G. M., Nicholson III, J., Brasseur, G., De Rudder, A., Schmailzl, U., and Pitts, M.: Detection of stratospheric HNO₃ and NO₂ response to short-term solar ultraviolet variability, Nature, 322, 43–46, doi:10.1038/322043, 1986.

López-Puertas, M., Funke, B., Gil-López, S., von Clarmann, T., Stiller, G. P., Höpfner, M., Kellmann, S., Fischer, H., and Jackman, C. H.: Observations of NO$_x$-Enhancements and Ozone Depletion in the Northern and Southern Hemispheres after the October-November 2003 Solar Proton Events, J. Geophys. Res., 110, A09S44, doi:10.29/2005JA011051, 2005.

Marsh, D. R., Solomon, S. C., and Reynolds, A. E.: Empirical model of nitric oxide in the lower thermosphere, J. Geophys. Res., 109, A07301, doi:10.1029/2003JA010199, 2004.

Newnham, D. A., Espy, P. J., Clilverd, M. A., Rodger, C. J., Seppälä, A., Maxfield, D. J., Hartogh, P., Holmén, K., and Horne, R. B.: Direct observations of nitric oxide produced by energetic electron precipitation into the Antarctic middle atmosphere, Geophys. Res. Lett., 38, L20104, doi:10.1029/2011GL048666, 2011.

Porter, H. S., Jackman, C. H., and Green, A. E. S.: Efficiencies for production of atomic nitrogen and oxygen by relativistic proton impact in air, J. Chem. Phys., 65, 154–167, 1976.

Renard, J.-B., Blelly, P.-L., Bourgeois, Q., Chartier, M., Goutail, F., and Orsolini, Y. J.: Origin of the January – April 2004 increase in stratospheric NO₂ observed in the northern polar latitudes, Geophys. Res. Lett., 33, doi:10.1029/2005GL025450, 2006.

Rusch, D. W., Gerard, J.-C., Solomon, S., Crutzen, P. J., and Reid, G. C.: The effect of particle precipitation events on the neutral and ion chemistry of the middle atmosphere, 1. Odd nitrogen, Planet. Space Sci., 29, 767–774, 1981.

Sinnhuber, M., Nieder, H., and Wieters, N.: Energetic Particle Precipitation and the Chemistry of the Mesosphere/Lower Thermosphere, Surv. Geophys., Springer Netherlands, Dordrecht, doi:10.1007/s10712-9201-3, 2012.

Sinnhuber, M., Funke, B., von Clarmann, T., López-Puertas, M., and Stiller, G. P.: Variability of NO$_x$ in the polar middle atmosphere from October 2003 to March 2004: vertical transport versus local production by energetic particles, Atmos. Chem. Phys. Disc., 14, 1–29, doi:10.5194/acpd-14-1-2014, 2014.

Siskind, D., Barth, C. A., and Roble, R.: The response of thermospheric nitric oxide to an auroral storm, 2. Auroral latitudes, J. Geophys. Res., 94, 16899–16911, doi:10.1029/JA094iA12p16899, 1989.

Solomon, S. C., Barth, C. A. and Bailey, S. M.: Auroral production of nitric oxide measured by the SNOE satellite, Geophys. Res. Lett., 26, 1259–1262, 1999.

Turunen, E., Verronen, P. T., Seppälä, A., Rodger, C. J., Clilverd, M. A., Tamminen, J., Enell, C.-F., and Ulich, T.: Impact of different energies of precipitating particles on NO$_x$ generation in the middle and upper atmosphere during geomagnetic storms, J. Atmos. Sol. Terr. Phys., 71, 1176–1189, doi:10.1016/j.jastp.2008.07.005, 2009.

Verronen, P. T., Rodger, C. J., Clilverd, M. A., and Wang, S.: First evidence of mesospheric hydroxyl response to electron precipitation from the radiation belts, J. Geophys. Res., 116, D07307, doi:10.1029/2011JD014965, 2011.

von Clarmann, T., Glatthor, N., Grabowski, U., Höpfner, M., Kell-
     mann, S., Kiefer, M., Linden, A., Mengistu Tsidu, G., Milz, M.,
     Steck, T., Stiller, G. P., Wang, D. Y., Fischer, H., Funke, B.,
     Gil López, S., and López-Puertas, M.: Retrieval of tempera-
     ture and tangent altitude pointing from limb emission spectra
     recorded from space by the Michelson Interferometer for Passive
     Atmospheric Sounding (MIPAS), J. Geophys. Res., 108, 4736,
     doi:10.1029/2003JD003602, 2003.

von Clarmann, T., Funke, B., López-Puertas, M., Kellmann, S., Lin-
     den, A., Stiller, G. P., Jackman, C. H., and Harvey, V. L.: The so-
     lar proton events in 2012 as observed by MIPAS, Geophys. Res.
     Lett., 40, 2339–2343, doi:10.1002/grl.50119, 2013.
von Storch, H. and Zwiers, F. W.: Statistical Analysis in Climate Re-
     search, Cambridge Univ. Press, Cambridge, UK, 378–380, 2001.